

Article

Provenance Analysis of the Paleogene Strata in the Northern Qaidam Basin, China: Evidences from Sediment Distribution, Heavy Mineral Assemblages and Detrital Zircon U-Pb Geochronology

Jianguo Yin ¹, Shuai Zhang ^{2,*} and Zhixiong Wu ³

¹ Key Laboratory of Petroleum Resources, Gansu Province/Northwest Institute of Eco-Environment and Resources, Chinese Academy of Sciences, Lanzhou 730000, China; yinjianguo@nieer.ac.cn

² Oil and Gas Survey, China Geological Survey, Beijing 100083, China

³ Research Institute of Exploration and Development, PetroChina Qinghai Oilfield Company, Dunhuang 736202, China; wzx19842003@163.com

* Correspondence: zhangshuai870517@163.com

Received: 31 August 2020; Accepted: 24 September 2020; Published: 27 September 2020



Abstract: Using provenance analysis to build an accurate source-to-sink relationship is the key to infer mountain building scenarios around the Qaidam Basin, and also important to understanding the uplift and expansion of the Tibetan Plateau. However, some conflicting provenance inferences are caused by different interpretations for the prevalent existence of the late Paleozoic to early Mesozoic age group in detrital zircon U-Pb age spectra of the Paleogene strata at the northern Qaidam Basin, and these need to be resolved. In this article, an integrated study of sediment distribution, heavy mineral assemblages, and detrital zircon U-Pb geochronology is carried out to analyze provenance of the Paleogene strata at the northern Qaidam Basin. The decreasing trends of the net sand to gross thickness ratios and conglomerate percentages away from the Qilian Mountains and Altyn Tagh range to basin interior clearly support they are the provenance areas. Sedimentation of materials from the Altyn Tagh range is spatially confined to a small area in front of the mountains. A large sandy body with a uniform distribution of detrital zircon ages (containing a lot of the late Paleozoic to early Mesozoic zircon ages) and heavy mineral assemblages in the Xiaganchaigou Formation is supplied by the Qilian Mountains.

Keywords: provenance analysis; stratigraphic thicknesses; net sand to gross thickness ratio; conglomerate percentage; heavy mineral analysis; detrital zircon U-Pb geochronology; Intermontane basin

1. Introduction

Tectonic activities of the northwestern Tibetan Plateau provide significant evidence for understanding the formation and evolution of the Tibetan Plateau. As the largest Cenozoic intermontane basin in the northwestern Tibetan Plateau, the Qaidam Basin accumulates a thick and continuous sedimentary succession and thus preserves important information to infer tectonic activities of its surrounding orogenic belts. Using provenance analysis to construct a reasonable source-to-sink relationship is the prerequisite to interpret the information of the sedimentary archive.

Numerous approaches have been applied to provenance analysis in the Qaidam Basin, including clast composition of conglomerate [1–3], sandstone modal analysis [4–7], detrital mineral U-Pb geochronology [8–13], paleocurrent analysis [3,4,10–13], heavy mineral analysis [4,5,14–16], and element geochemistry [7,17], etc. However, some discrepancies still exist in previous results of provenance analysis. Bush et al. (2016) [4] thought that a long E-directed drainage system transported materials

eroded from the eastern Kunlun Mountains to the Dahonggou area (the Dhg in Figure 1c) and formed the Lulehe Formation (Fm.) in this area. Wang et al. (2017) [13] also suggested that the eastern Kunlun Mountains was the dominant provenance of the Lulehe and Xiaganchaigou Fms. in the Dahonggou area. Song et al. (2019) [12] pointed out the Altyn Tagh range was the provenance of the upper Lulehe, Xiganchaigou, and lower Shangganchaigou Fms. in the Dahonggou area. Lu et al. (2018) [11] and Zhuang et al. (2011) [3] thought the Lulehe Fm. in the Dahonggou area had a proximal northerly source area. The conflicting provenance inferences were mainly based on paleocurrent measurement and detrital zircon U-Pb geochronology from outcrops. The former is easily influenced by the high sinuosity of rivers, while the latter is easily influenced by the high complexity of rock types and ever-changing catchment area in provenance. When the paleocurrent only represents flow direction of one specified river reach but the entire drainage system, determining the provenance by comparisons of detrital zircon U-Pb age spectra may be error-prone and need more caution. The proportion variation of the late Paleozoic to early Mesozoic age group in detrital zircon U-Pb age spectra of the Paleogene strata in the Dahonggou area is the important evidence applied to analyze provenance in the above-mentioned articles and also the main factor to cause the conflicting provenance inferences. The controversy of provenance analysis refers to different tectonic geomorphology and mountain building scenarios for the orogenic belts surrounding the Qaidam Basin and need to be resolved.

The Qaidam Basin has been an endorheic intermontane basin in the Cenozoic [11]. The trunk rivers formed by confluence of the tributaries in the mountainous catchment areas flow through apex or intersection points and then become distributive drainage systems in the basin [18]. Without intensive impaction of the axial rivers, the resulted sedimentary bodies commonly show downstream decrease in channel proportion, channel scale and grain size [19], etc. Therefore, the regional sediment distribution (e.g., stratigraphic thicknesses, net sand-to-gross thickness (NTG) ratios, and conglomerate percentages, etc.) can be used to infer the delivery pathways of sediments. The sediment delivery pathways obtained from the sediment distribution trends are more representative than paleocurrent data of sparse outcrops. Although the stratigraphic information from sparse outcrops at the basin margin is not enough to acquire the regional changes in trends, the decades-long petroleum exploration and exploitation activities of the PetroChina Qinghai Oilfield Company have accumulated large amounts of drilled well data and make regional analyses of sediment distribution possible.

In this study, we analyzed the regional changes in trends of stratigraphic thicknesses, NTG ratios and conglomerate percentages in the northern Qaidam Basin. Heavy mineral analysis and detrital zircon U-Pb geochronology of nine samples were also conducted to infer the provenance. These results show that the provenance of the Paleogene strata in the northern Qaidam Basin is from the neighbouring Altyn Tagh range and Qilian Mountains, and that materials from the Altyn Tagh range are not southwardly transported to the Dahonggou area.

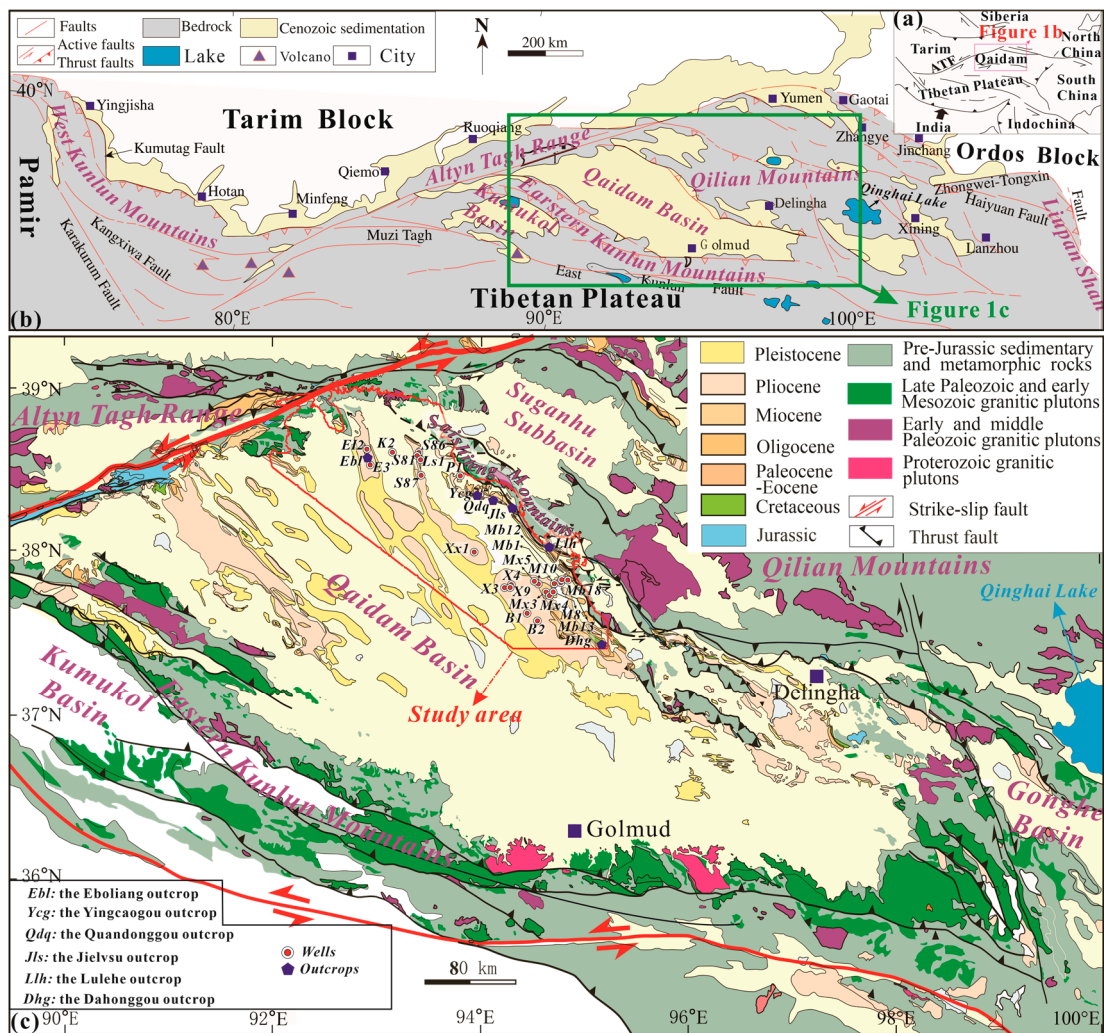


Figure 1. (a) Sketch map of the Tibetan Plateau and adjacent regions, showing the major faults. (b) Regional tectonic map around the Qaidam Basin located at the northeastern margin of the Tibetan Plateau (modified from Wang et al. 2015 [20]). (c) Detailed geological map of the study area in the northern Qaidam Basin (modified from Cheng et al. 2019a [21]).

2. Geological Background

The Qaidam Basin, which is an intermontane basin surrounded geographically by the Altn Tagh Range to the northwest, the Qilian Mountains to the northeast, and the eastern Kunlun Mountains to the south (Figure 1), is the largest petroliferous basin in the Tibetan Plateau and infilled by thick Cenozoic strata atop the Jurassic, Cretaceous, or the basement.

2.1. Stratigraphy

These Cenozoic strata in the Qaidam Basin have been subdivided into seven stratigraphic units, including the Lulehe, Xiaganchaigou, Shangganchaigou, Xiayoushahan, Shangyoushahan, Shizigou, and Qigequan Fms. The forming ages of these strata have been previously delineated by ostracods, fossil mammals, lithostratigraphic correlations, and magnetostratigraphy [22–27]. The stratigraphic chronologies of the Cenozoic strata derived from the Dahonggou section by Wang et al. (2017) [13] is in conflict with other regional chronologies in the Qaidam Basin [28] and not adopted in this article. A more widely accepted division scheme of stratigraphic chronologies is that the Lulehe Fm. is 53.5–43.8 Ma [25,27,29], the Xiaganchaigou Fm. is 43.8–35.5 Ma [24,25,27], the Shangganchaigou Fm. is 35.5–22 Ma [22,24,25], the Xiayoushahan Fm. is 22–15.3 Ma [22–24], the Shangyoushahan Fm. is

15.3–8.1 Ma [23], the Shizigou Fm. is 8.1–2.5 Ma [23,24], and the Qigequan Fm. is 2.5–0 Ma [23]. The Paleogene strata, consisting of the Lulehe, Xiaganchaigou, and Shangganchaigou Fms., are easily distinguished from each another by the lithology in the northern margin outcrops of the Qaidam Basin [3,13]. This difference of lithology is the key foundation for tracing stratigraphic units from one location to another by subsurface data. The stratigraphic correlation of subsurface data is successfully built by the PetroChina Qinghai Oilfield Company.

2.2. Geochronological Characteristics of Potential Provenances of the Paleogene Strata in the Northern Qaidam Basin

In this article, detrital zircon U-Pb ages are used to infer the provenance evolution of the Paleogene strata in the northern Qaidam Basin. The zircon U-Pb age spectra of three potential provenances, namely the Qilian Mountains, the Altyn Tagh Range, and the eastern Kunlun Mountains, can be distinguished from one another is the prerequisite for applying this method. The characteristics of zircons sourced from the three provenance candidates are presented in Figure 2 [9].

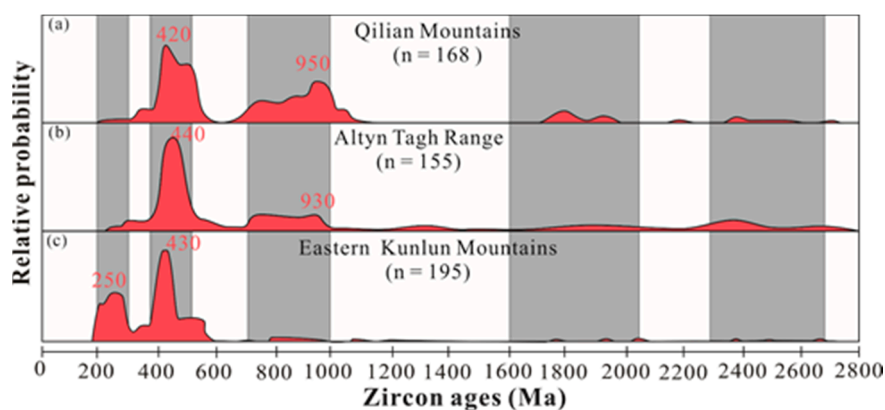


Figure 2. The relative probability plots of zircon U-Pb ages [9] from (a) basement rocks in the Qilian Mountains, (b) basement rocks in the Altyn Tagh Range and (c) basement rocks in the Eastern Kunlun.

The Qilian Mountains, located between the North Qilian Suture Zone and the North Qaidam ultrahigh-pressure metamorphic rocks (UHP Belt), mainly consists of a Precambrian crystalline basement overlain by thick and large-area Paleozoic sedimentary strata [30–33]. Additionally, forming-ages of granitoids outcropped in the Qilian Mountains adjacent to the northern Qaidam Basin margin are dominantly early Paleozoic [30,34]. In addition, a few late Paleozoic–early Mesozoic granitoids are exposed in the Saishiteng Mountains, northwestern part of the Qilian Mountains (Figure 1c) [13]. Relative probability plots of zircon U-Pb ages from basement rocks and magmatic intrusives of the Qilian Mountains are shown in Figure 2a [9] and indicate that zircons with early Paleozoic and Neoproterozoic ages are dominant. In addition, the Permian–Jurassic sedimentary rocks in the Qilian Mountains commonly have a major peak of late Paleozoic–early Mesozoic ages (200–300 Ma) in detrital zircon age spectra [35–37]. The late Paleozoic–early Mesozoic-aged zircons in the Permian–Jurassic sedimentary rocks are believed to originally be shed from the eastern Kunlun Mountains [4,35,36].

The basement rocks of the Altyn Tagh Range consist of the Archean–late Paleozoic magmatic rocks with zircon ages spanning from ~3.6 Ga to ~260 Ma [30,31]. In particular, the Early Paleozoic felsic rocks are widely distributed in the Altyn Tagh Range (Figure 2b) [31,37,38]. Additionally, several Permian plutonic terranes are exposed in the central part of the range (Figure 1c) [31] and make the late Paleozoic age as a major peak in detrital zircon U-Pb age spectra of the Cenozoic strata in the adjacent Eboliang outcrop (Figure 7 in Cheng et al., 2016 [9]).

The late Paleozoic–early Mesozoic granitoids outcrop widely in the Eastern Kunlun Mountains, making 200–300 Ma one of two major age groups in the zircon U-Pb age spectrum of the East Kunlun

Shan (Figure 2c). The late Paleozoic–early Mesozoic granitoids record magmatic events related to the Paleo-Tethyan tectonic regime [39–41]. The early Paleozoic age group is the other major age group. The early Paleozoic tectono-magmatic events are comparable to the Qilian orogenic belt and constituent part of the Qilian-Kunlun Caledonian orogenic system [32,41]. Compared to the late Paleozoic–early Mesozoic and early Paleozoic ages, the Precambrian ages are rare [8,13] in the eastern Kunlun Mountains, although the Proterozoic rocks are exposed in both the eastern Kunlun Mountains and the Qilian Mountains [41].

3. Materials and Methods

In this study, well cuttings from 147 drilled wells were collected to calculate the stratigraphic thicknesses, NTG ratios and conglomerate percentages of the Lulehe, Xiaganchaigou and Shangganchaigou Fms. For each of these stratigraphic units, calculation only applies data from wells drilling through the corresponding unit. The wells with missing stratigraphic units are abandoned, too. Accordingly, 96, 123 and 122 in the 147 wells are finally available for the calculation of the Lulehe, Xiaganchaigou and Shangganchaigou Fms, respectively. The NTG ratio represents thickness ratio of conglomerates, sandstones and siltstones to stratigraphic unit in an individual drilled well. The conglomerate percentage represents ratio of the thickness of conglomerates, gravelly clastic rocks multiplied by a factor of 0.4 and gravel-bearing clastic rocks multiplied by a factor of 0.1 to the stratigraphic unit. According to the gravel contents in conglomerates (more than 30%), gravelly clastic rocks (between 5–30%) and gravel-bearing clastic rocks (less than 5%), the above two factors are chosen to transfer the thickness of gravelly clastic rocks and gravel-bearing clastic rocks to conglomerates.

Additionally, eleven sandstone samples collected from 8 cored wells were prepared for heavy mineral analysis and detrital zircon U-Pb dating (Table 1; Figure 1c). Separation, concentration, and identification of heavy minerals were performed at the Institute of Regional Geological Survey of Hebei Province, Langfang, Hebei Province, China by following the procedures outlined by Mange and Maurer (1992) [42] and Liu et al. (2013) [43]. Zircons (ca. 300 grains) were mounted in epoxy resin and then polished to obtain a smooth surface. Reflected and transmitted light as well as cathodoluminescence (CL) images were obtained to pick suitable dating targets, avoiding inclusion and cracks. Zircon U-Pb dating was carried out on Agilent 7200 ICP-MS combined with a Photon-machines Analyte Exite 193 nm laser ablation system at Lanzhou University (Lanzhou, China). In addition, ca. 80–100 effective zircon ages should be acquired to achieve statistically reliable detrital zircon U-Pb dating results. Zircon 91500, for which the preferred U-Pb isotopic ratios were found by Wiedenbeck et al. (1995) [44], was used as the external standard for U-Pb dating and was analyzed once every five analyses. The GLITTER 4.0 software was used to calculate the U-Pb isotope ratios and element contents. The U-Pb ages of detrital zircons younger than ca. 1000 Ma were calculated from $^{206}\text{Pb}/^{238}\text{U}$ ratios, whereas ages older than ca. 1000 Ma were calculated from $^{207}\text{Pb}/^{206}\text{Pb}$ ratios. Detrital zircon U-Pb ages with discordance degree >10% were excluded from the results. The probability density functions and histogram plots were plotted using the Isoplot 3.0 software [45]. A more detailed description of the sample separation methods and analytical procedures was given by Yuan et al. (2004) [46].

Table 1. Basic information of samples collected for heavy mineral analysis and detrital zircon U-Pb dating.

Samples	Depth (m)	Stratigraphic Units	Heavy Mineral Analysis	Zircon U-Pb Dating	Wells
B2u-s	3275	Xiaganchaigou Fm.	√	√	Well B2
B2d-s	3532	Xiaganchaigou Fm.	√	√	
Mx3-s	1240	Lulehe Fm.	√	√	Well Mx3
Mx4-s	1317	Lulehe Fm.	√	√	Well Mx4
Mx5u-s	1940	Xiaganchaigou Fm.	√	√	Well Mx5
Mx5d-s	2287	Lulehe Fm.	√	√	
X4-s	1806	Shangganachaigou Fm.	√	√	Well X4
Xx1u-s	4115	Xiaganchaigou Fm.	√	√	Well Xx1
Xx1d-s	4852	Lulehe Fm.	√	√	
Mb13-s	1450	Xiaganchaigou Fm.	√		Well Mb13
Mb18-s	1553	Xiaganchaigou Fm.	√		Well Mb18

4. Results

4.1. Sediment Distribution

Data of the stratigraphic thickness, NTG ratios and conglomerate percentages from drilled wells are listed in Supplementary Table S1. The drilled wells are presented in Supplementary Figure S1.

The thicknesses of the Lulehe Fm. are mainly less than 650 m (Figure 3a). A paleohigh is at southeastern margin of the study area, and some local sub-depocenters are near basin margin and show basinward thinning of thicknesses (Figure 3a). The NTG ratios of the Lulehe Fm. show basinward decrease (Figure 3b). The lowest NTG ratios are in the northwestern study area and far away from basin margin. The local sub-depocenters have relatively high NTG ratios and conglomerate percentages (Figure 3b,c). The conglomerate percentages of the Lulehe Fm. present the same trend as the NTG ratios (Figure 3c).

The thicknesses of the Xiaganchaigou Fm. are apparently increased and present basinward increasing trend (Figure 3d). The paleohigh at southeastern margin of the study area is covered by the Xiaganchaigou Fm., and a large depocenter is formed in the northwestern study area (Figure 3d). This depocenter has lowest NTG ratios (Figure 3e). The NTG ratios present decreasing trend from basin margin to the depocenter (Figure 3e). The conglomerate percentages of the Xiaganchaigou Fm. still present basinward decrease (Figure 3f). Compared to the Lulehe Fm., the conglomerate percentages of the Xiaganchaigou Fm. are lower, especially at eastern margin of the study area (Figure 3c,f). According to the isopach map and NTG ratios distribution, a large-scale sandy body is believed to be formed in southern study area (Figure 3d,e).

The thicknesses of the Shangganachaigou Fm. are obviously decreased and present basinward increasing trend (Figure 3g). The white parts in the study area are areas where the Shangganachaigou Fm. is completely removed after the later uplift (Figure 3g; Figure 11 in Cheng et al., 2016 [9]). There are two sub-depocenters formed in northwestern and central areas (Figure 3g). The NTG ratios present decreasing trend away from basin margin to the depocenters (Figure 3h). In the northern study area, the conglomerate percentages of the Shangganachaigou Fm. are larger than that of the Shangganachaigou Fm. (Figure 3f,i). Nevertheless, the former still maintains similar plane distribution characteristics of the latter (Figure 3f,i).

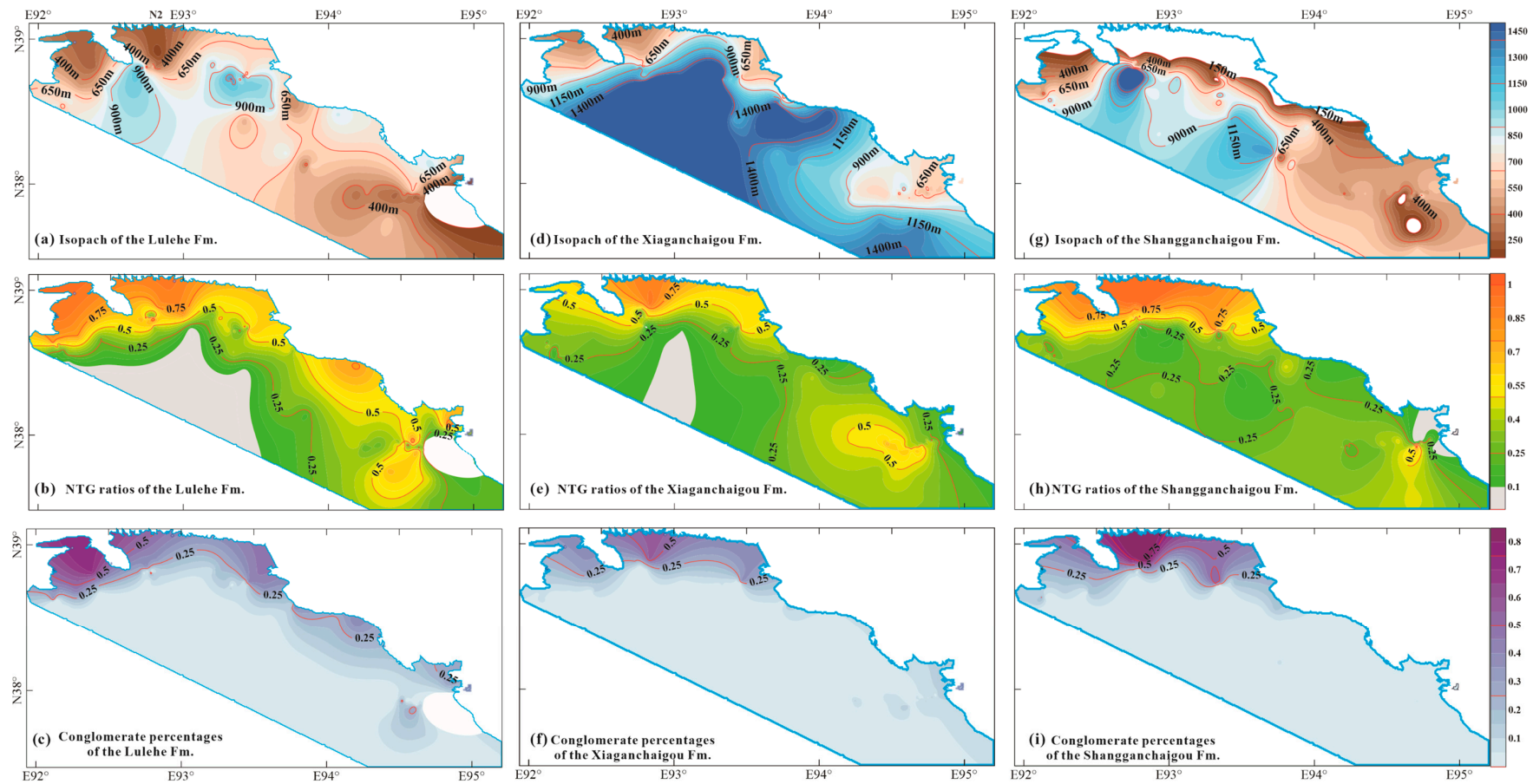


Figure 3. The plane distribution of stratigraphic thicknesses, NTG ratios and conglomerate percentages of the Paleogene strata. White area in study area represents area missing stratum. (a) Isopach of the Lulehe Fm. (b) NTG ratios of the Lulehe Fm. (c) Conglomerate percentages of the Lulehe Fm. (d) Isopach of the Xiaganchaigou Fm. (e) NTG ratios of the Xiaganchaigou Fm. (f) Conglomerate percentages of the Xiaganchaigou Fm. (g) Isopach of the Shangganchaigou Fm. (h) NTG ratios of the Shangganchaigou Fm. (i) Conglomerate percentages of the Shangganchaigou Fm.

4.2. Heavy Mineral Analysis

The heavy mineral analysis data are listed in Supplementary Table S2. Except for heavy mineral analysis data of wells B2, X4, Mx3, Mx4, Mx5, and Xx1, others are cited from Jian et al., 2013 [5]. Fe-oxide minerals (i.e., magnetite, hematite, and limonite) are excluded in heavy mineral analysis due to their susceptibility to hydraulic-sorting [47], so heavy mineral analysis data from Jian et al., 2013 [5] are renormalized and also listed in Supplementary Table S2. Drilled wells with heavy mineral assemblages are plotted to present the plane dissimilarities and similarities (Figure 4).

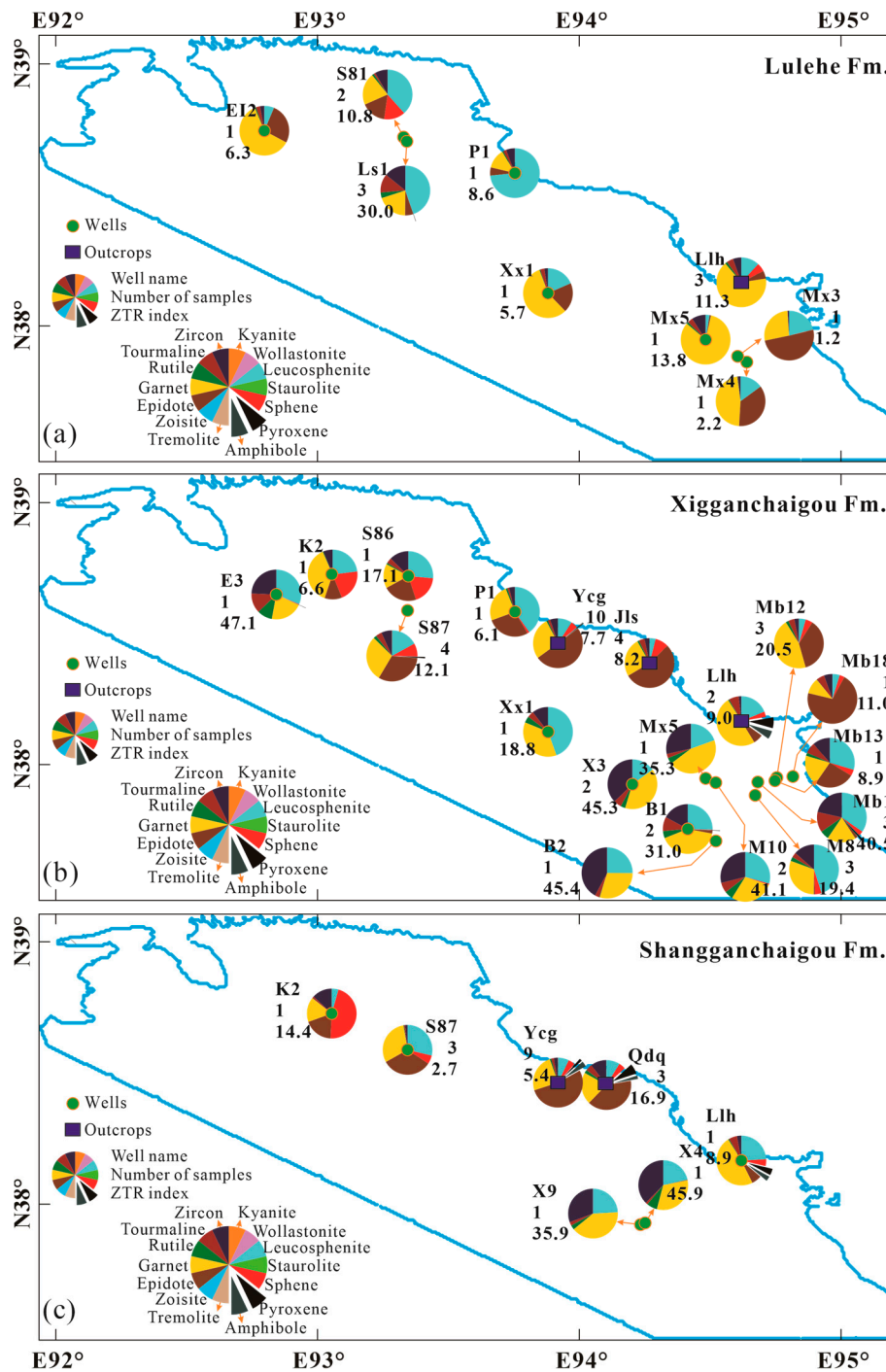


Figure 4. The characteristics of the heavy mineral assemblages of the Paleogene strata. (a) Lulehe Fm. (b) Xigganchaigou Fm. (c) Shangganchaigou Fm.

In the Lulehe Fm. (Figure 4a), the heavy mineral assemblages of Mx4 and Mx3 are similar, consist dominantly of epidote, garnet and leucosphenite, and display a very low abundance of ZTR minerals (zircon, tourmaline and rutile). Garnet is the dominant mineral species of Mx5 and Llh. S81 consists of ZTR minerals, garnet, epidote, sphene (titanite), and leucosphenite, and is different from near Ls1, which consists of ZTR minerals, garnet, and leucosphenite. P1 has the same heavy mineral types of Ls1 but is dominated by leucosphenite, accompanied by minor ZTR minerals, garnet and epidote.

In the Xiaganchaigou Fm. (Figure 4b), the heavy mineral assemblages of Xx1 and Mx5 are quite different from that of the Lulehe Fm., and consist dominantly of ZTR minerals, garnet, and leucosphenite. M1, M8, M10, B1, B2, and X3 have the same heavy mineral assemblages as Xx1 and Mx5. Ycg and Jls have similar heavy mineral assemblages composed dominantly of epidote and garnet. Epidote and garnet of P1 increase obviously. The heavy mineral assemblages of K2, S86 and S87 consist of ZTR minerals, garnet, epidote, sphene and leucosphenite, and are similar to S81 of the Lulehe Fm. Compared to Lulehe Fm., minor amphibole and pyroxene are showed in Llh. Ycg and Jls are similar and consist dominantly of epidote and garnet.

In the Shangganchaigou Fm. (Figure 4c), X9 and X4 (near X3) still consist dominantly of ZTR minerals, garnet and leucosphenite. Heavy mineral assemblages of Llh and S87 have no obviously change. Sphene of K2 increases obviously. Minor amphibole and pyroxene are showed in Ycg, which still consist dominantly of epidote and garnet. Qdq is very similar to Ycg.

4.3. Zircons Dating Results

The detrital zircon U-Pb dating results are listed in Supplementary Table S3. The Th/U ratios of the analyzed zircons are generally greater than 0.1 and indicative of the predominant magmatic origin (Figure 5) [48]. The detrital zircon U-Pb ages of the nine samples can be statistically subdivided into three groups: the Precambrian, spanning from ca. 2800 Ma to 550 Ma (peaks at ca. 800–900 Ma, ca. 1700–1800 Ma, and ca. 2300–2500 Ma), early to middle Paleozoic (peaks at ca. 410–450 Ma), and late Paleozoic to early Mesozoic (peaks at ca. 230–270 Ma) (Figures 5 and 6a–i). Except for sample Xx1d-s, the Precambrian zircons outnumber the late Paleozoic to Mesozoic zircons, and the peak height of the late Paleozoic to Mesozoic group increases with peak heights of the Precambrian group in detrital zircon age spectra (Figure 6a–i). The latter feature is even more obviously shown by the positive correlation between the “late Paleozoic to Mesozoic/early to middle Paleozoic zircons” ratio and the “Precambrian zircons/early to middle Paleozoic zircons” ratio (Figure 6j). Additionally, the above mentioned two features also can be observed in detrital zircon age spectra of the Cenozoic strata in the Dahonggou outcrop (Figure 11A in Bush et al., 2016 [4]).

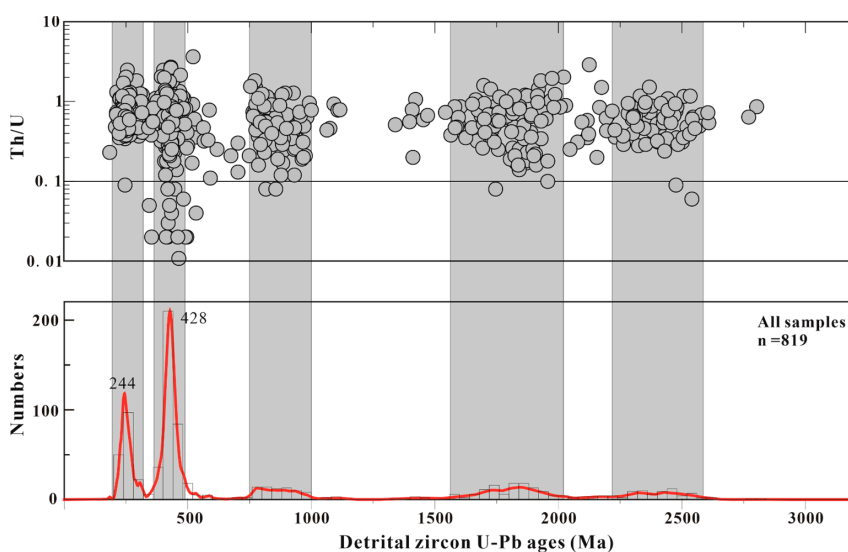


Figure 5. The Th/U ratios and detrital zircon ages of all analyzed samples.

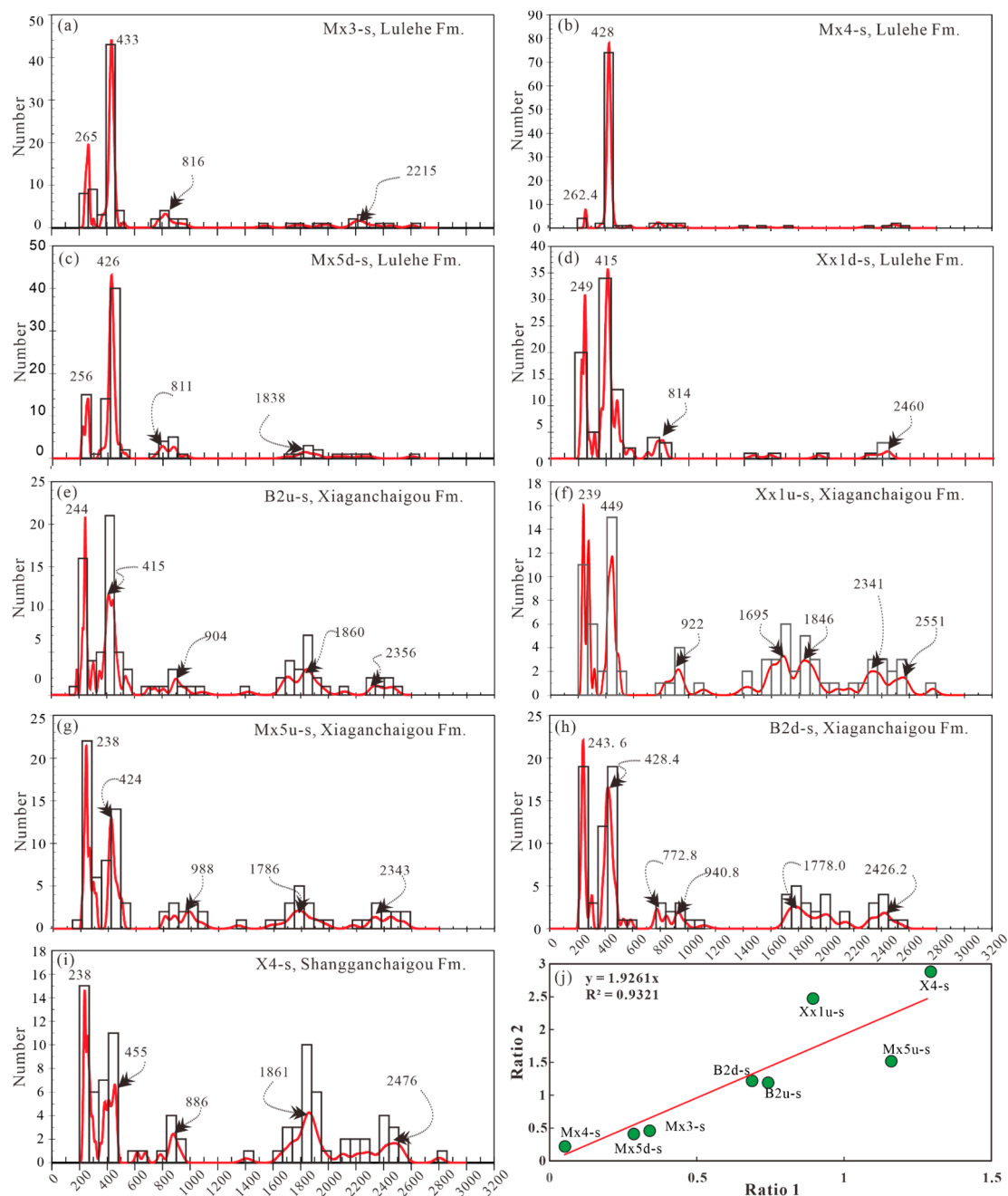


Figure 6. (a–i) Graphs of detrital zircon age spectra in study area. (j) Peaks height correlation between the Precambrian zircons and late Paleozoic to Mesozoic zircons. The ratio 1 represents “late Paleozoic to Mesozoic/early to middle Paleozoic zircons” ratio, and ratio 2 represents the “Precambrian zircons/early to middle Paleozoic zircons” ratio.

4.3.1. Samples from the Lulehe Fm.

Samples Mx5m-s, Mx3-s, and Mx4-s exhibit similar detrital zircon age spectra (Figure 6a–c), and the early to middle Paleozoic group is dominant in the spectra. The zircon ages in these three samples are distributed between 207 and 2608 Ma with a major ca. 430 Ma peak and minor peak at 260 Ma. The Precambrian group obtains three very low peaks at ca. 800 Ma, ca. 1800 Ma, and ca. 2200 Ma in these three samples.

The zircon ages in sample Xx1d-s are distributed between 211 and 3353 Ma. The zircon of 3353 Ma is obviously older than other zircons of all samples and is not shown in Figure 6d. The zircon ages in

sample Xx1d-s mainly consist of early to middle Paleozoic group (peaks at 415 Ma) and late Paleozoic to Mesozoic group (peaks at 249 Ma) (Figure 6d). The Precambrian group only shows a low peak at 814 Ma and 2460 Ma (Figure 6d). This implies that the provenance of sample Xx1d-s differs from that of samples Mx5m-s, Mx3-s, and Mx4-s.

4.3.2. Samples from the Xiaganchaigou Fm.

Samples B2u-s, B2d-s, Mx5u-s, and Xx1u-s were collected from the Xiaganchaigou Fm. These four samples exhibit very similar detrital zircon age spectra (Figure 6e–h). The early to middle Paleozoic group and late Paleozoic to Mesozoic group are shown as two major peaks in detrital zircon age spectra (Figure 6e–h). The early to middle Paleozoic group peaks at ca. 410–450 Ma, and the late Paleozoic to Mesozoic group peaks at ca. 240 Ma. The Precambrian group exhibits three minor peaks at ca. 800–900 Ma, ca. 1700–1800 Ma, and ca. 2300–2500 Ma.

4.3.3. Samples from the Shangganchaigou Fm.

Sample X4-s was collected from the Shangganchaigou Fm. The detrital zircon age spectrum of the sample is the same as that of samples from the Xiaganchaigou Fm (Figure 6i).

5. Discussion

5.1. Provenance Analysis of the Lulehe Fm.

The decrease in trends of the NTG ratios and conglomerate percentages from the Altyn Tagh Range, Saishiteng Mountains and Qilian Mountains to basin interior imply that the Lulehe Fm. is sourced from these mountains (Figure 3b,c). Sandy bodies are mainly deposited in piedmont areas of these mountains and thus deny the existence of long axial rivers sourced from either the Altyn Tagh Range or the eastern Kunlun Mountains in this study area (Figure 3b). Widely deposited alluvial fans in front of these mountains, in which poorly sorted debris deposits (e.g., brownish-red matrix-supported conglomerates and muddy gravelly sandstones) are largely reserved, also support nearby provenances (Figure 7a) [49]. The plane distribution of sedimentary facies, presented by transition of the alluvial fans at basin margin to alluvial plain and lacustrine toward the basin interior, also suggests that sediments are delivered away from these mountains [49]. The published paleocurrent data observed from the Jls (southwest-directed flow [3]; named as Lake Mahai in Zhuang et al., 2011 [3]), Lulehe (southwest-directed flow [3]), and Dahonggou outcrops (southwest- or southeast-directed flow [4,12,50]) agree with delivery pathways of sediments from the Saishiteng Mountains and the Qilian Mountains. Isopach map shows that some local depocenters with relatively high NTG are developed close to basin margin and thin toward basin interior (Figure 3a). This may be ascribed to (1) local residue depressions caused by pre-Cenozoic tectonic inversion from extension to compression [51], (2) newly formed local depressions due to the Cenozoic tectonic events [52], and (3) clastic wedges of alluvial fans thinning away from sources [11].

According to the bedrock's outcrops in the Qilian Mountains adjacent to the northern Qaidam Basin, the detrital zircon ages eroded from the Qilian Mountains should consist dominantly of the early to middle Paleozoic ages (Figure 2a) [4,13,53]. The detrital zircon age spectra of samples Mx5m-s, Mx3-s, and Mx4-s are also dominated by the early to middle Paleozoic ages (Figure 6a–c). Thus, the zircons dating results support the provenance of the Lulehe Fm. of Wells Mx5, Mx3, and Mx4 is the Qilian Mountains. The difference of heavy mineral assemblages between Mx5, Mx3, and Mx4 can be explained by different catchment areas in the Qilian Mountains (Figure 4a). However, the detrital zircon age spectrum of sample Xx1d-s mainly consist of the early to middle Paleozoic ages and the nearly equivalent late Paleozoic to early Mesozoic ages (Figure 6d) and implies that sample Xx1d-s should have a different provenance. Though the Permian plutonic terranes are exposed in both the central part of the Altyn Tagh Range (Figure 1) [9,31] and the western Saishiteng Mountains (Figure 1c) [9,12],

the distinctive heavy mineral assemblages of Xx1d-s, the NTG ratios, and conglomerate percentages tends to support provenance from the Saishiteng Mountains.

Thus, we can reasonably conclude that the Qilian Mountains, the Saishiteng Mountains and the Altyn Tagh Range are the provenances of the Lulehe Fm. in the study area (Figure 7a). The inference is compatible with the Paleocene-early Eocene uplift of these mountains by virtue of detrital zircon fission track evidence [20], detrital apatite fission track evidence [54,55], and structural analysis of seismic sections and outcrops [52,56]. In the paleogeographic map of the Lulehe Fm., provenances and widely deposited alluvial fans are shown (Figure 7a).

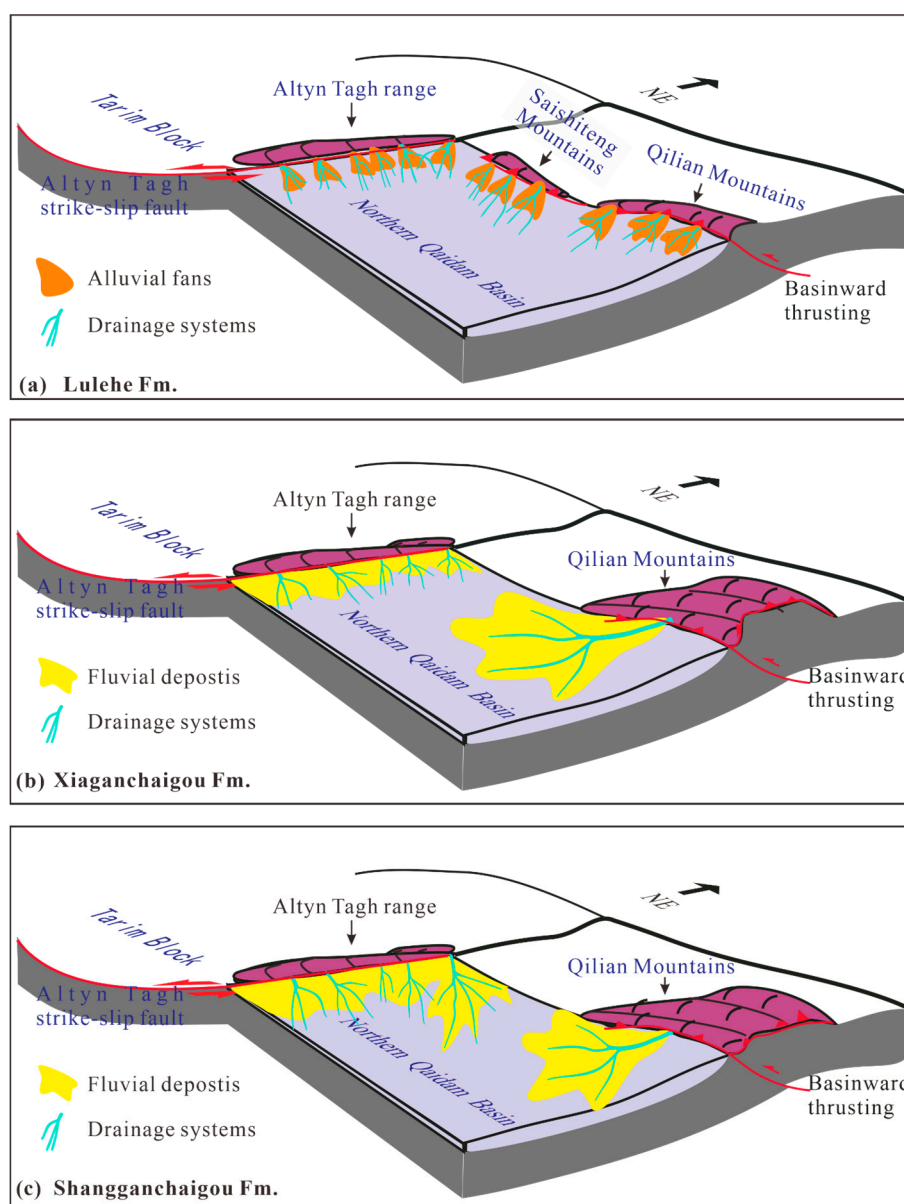


Figure 7. The paleogeographic maps of the Paleogene strata.

5.2. Provenance Analysis of the Xiaganchaigou Fm.

In the Xiaganchaigou Fm., a large depocenter is presented in the isopach map and located at central to northern study area (Figure 3d). Decreasing trends of the NTG ratios and conglomerate percentages from the Altyn Tagh Range and Qilian Mountains to the depocenter imply provenances from these mountains (Figure 3e,f). The low conglomerate percentages in front of the Qilian Mountains mean that the boundary between mountain and basin is further to the northeast (Figure 3f). The plane

appearances of the NTG ratios and isopach map are very similar, and the depocenter has the lowest NTG ratios (Figure 3e,f). The features are related to the downstream allocation of sediments and roughly approximate to the published plane distribution of fluvial-lacustrine facies [49]. However, the NTG ratios show two distinctive differences, including that (1) the low NTG ratios in front of the Saishiteng Mountains disagree with a proximal source area and (2) a large scale sandy body is deposited in southern study area and sourced from the Qilian Mountains (Figure 3d,e and Figure 7b). The former can be interpreted by that the paleohigh which was located in the Saishiteng Mountains and supplied materials to the Lulehe Fm. was no longer existed in the depositional period of the Xiaganchaigou Fm. The same situation is experienced by the paleohigh close to the southeastern margin of the study area (Figure 3a,e). The latter can be further proved by the evidence from the heavy mineral assemblages and detrital zircon U-Pb dating, which present obvious differences in comparison with the Lulehe Fm (Figure 4b).

Wells in the area covered by the large scale sandy body (e.g., Xx1, X3, Mx5, M1, M8, M10, B1, and B2) have the same heavy mineral assemblages composed dominantly of ZTR minerals, garnet and leucosphenite, and are different from wells in front of the Altyn Tagh range (e.g., E3, K2, S86, and P1) (Figure 4b; Supplementary Figure S1; Figure 3d,e), suggesting they have the same provenance. Samples B2u-s, B2d-s, Mx5u-s, and Xx1u-s of the Xiaganchaigou Fm. collected from some of these wells exhibit highly similar detrital zircon age spectra characterized by two major peaks of the early to middle Paleozoic group and late Paleozoic to early Mesozoic group and some minor peaks of the Precambrian group, and also suggest they have the same provenance. Additionally, detrital zircon age spectra of the Xiaganchaigou Fm. from wells Mb18, Mb17 (Figure 3 in Wang et al., 2019 [57]) and the nearby Dahonggou outcrop have the same characteristics (Figure 11 in Bush et al., 2016 [4]). The large scale sandy body with uniform distribution of detrital zircon ages and heavy minerals assemblages that are sourced from the Qilian Mountains may implies a large catchment area is formed in the mountains. Such a catchment area is needed to provide enough sediments with uniformly mixed provenance signals [58].

The presence and absence of the late Paleozoic to early Mesozoic age group has been used as important evidence to infer provenance [4,12,13]. When the late Paleozoic to early Mesozoic zircons are presented as a major peak in age spectra of clastic rocks, the Qilian Mountains, in which the Permian–Triassic plutonic terranes are rarely exposed, is commonly excluded from the provenances in previous works [12,13]. However, the late Paleozoic and Mesozoic sedimentary strata are widely distributed in the Qilian Mountains and can supply considerable the late Paleozoic to early Mesozoic zircons [11,37]. Considering that the NTG ratios and conglomerate percentages distribution indicate a delivery path of sediments away from the Qilian Mountains (Figure 3e,f), the late Paleozoic to early Mesozoic zircons should be sourced from the recycled late Paleozoic and Mesozoic sedimentary strata in the Qilian Mountains. The age spectra of clastic rocks show that the late Paleozoic to Mesozoic group increases with the Precambrian group (Figure 6j), which is a significant constituent in age spectra of the Qilian Mountains [37], and further supports this view. In addition, the spectra of these samples are obviously different from those of the Cenozoic clastic rocks [9] and modern sediments [12] sourced from the Altyn Tagh range.

Thus, we can reasonably conclude that the Qilian Mountains and the Altyn Tagh Range are the provenances of the Lulehe Fm, and that materials eroded from the Altyn Tagh Range and the eastern Kunlun Mountains have not been delivered to the southern study area (Figure 7b). The inference is consistent with the previous works [4,5]. The southwest-directed paleoflow from the Dahonggou outcrop reveals a transverse dispersal away from the Qilian Mountains in the Xiaganchaigou Fm. [4]. Jian et al. (2013) [5] concluded that the Altyn Tagh Range and Qilian Mountains were the potential provenance of the northern Qaidam Basin in the Paleogene and Neogene via the integrated analysis of framework petrography, heavy mineral analysis, and mineral chemistry. Materials of Wells B2, Mx5, X4, Mb17, Mb18, and Xx1 (located at depositional area A in Jian et al., 2013 [5]) are sourced from the Qilian Mountains. The materials from Altyn Tagh Range are only deposited at its front

area [20] and blocked by the depocenter to transport onwards to the southern study area (Figure 3d, Figure 7b). The detrital apatite fission-track data from the Jiuquan Basin [59] and Qaidam Basin [54] both point to the rapid exhumation of the Qilian Mountains during the middle-late Eocene (~42–38 Ma). The apatite fission-track data of in situ bedrocks in the Qilian Mountains also reveal this rapid cooling event [60]. Zhuang et al. (2011) [3] propose the uplifted area in the Qilian Mountains experiences regional expansion during the depositional period of the Xiaganchaigou Fm. by detailed sedimentary analysis of outcrops. Intensive uplift and expansion of the uplifted area in the Qilian Mountains make formation of the large scale sandy body possible (Figure 7b).

5.3. Provenance Analysis of the Shangganhaigou Fm.

The NTG ratios present a decreasing trend away from the Altyn Tagh range and the Qilian Mountains to the two sub-depocenters at northwestern and central study areas and imply the Shangganhaigou Fm. is sourced from these mountains (Figure 3h,i; Figure 7c). Thus, the decreasing thicknesses are ascribed to the weaker tectonic activities of these mountains during deposition of the Shangganhaigou Fm. According to the distribution of NTG ratios and conglomerate percentages, the sedimentary bodies in front of the Altyn Tagh range and the Qilian Mountains exhibit progradation and retrogradation, respectively (Figure 3h,i; Figure 7c). This feature can be interpreted by interaction between decreasing accommodation and sediments supply under the control of weakened tectonic activities. Bao et al. (2017) [61] agreed that a relatively stable tectonic setting caused the low sediment flux in the Shangganhaigou Fm. He et al. (2018) [54] also considered that the Qilian Mountains did not experience rapid exhumation in the Shangganhaigou Fm. The heavy mineral assemblages of wells X9, X6, and X4 are also composed dominantly of ZTR minerals, garnet and leucosphenite, and suggest they are sourced from the Qilian Mountains (Figure 4c; Figure 7c). The good similarity of the detrital zircon age spectrum of sample X4-s with that of samples from the Xiaganchaigou Fm. further supports that the Qilian Mountains is still the provenance area (Figure 6i). The paleocurrent data observed from the Jls (northwest-directed flow [3]), Lulehe (northwest-directed flow [3]), and Dahonggou outcrops (southwest-directed flow [4,50]) suggest that the Qilian Mountains continuously supplied material into the Qaidam Basin in the Shangganhaigou Fm. Thus, the Shangganhaigou Fm. is still sourced from the Altyn Tagh range and Qilian Mountains and exhibits progradation and retrogradation in front of these mountains, respectively (Figure 7c).

6. Conclusions

In this article, the provenance of the Paleogene strata in the northern Qaidam Basin is inferred by virtue of evidence from sediment distribution, heavy mineral assemblages, and detrital zircon U-Pb dating. The main conclusions are as follows.

(1) The decreasing trends of the NTG ratios and conglomerate percentages away from the Qilian Mountains and Altyn Tagh range obviously support the fact that they are provenance areas of the Paleogene strata. The sandy bodies sourced from the Altyn Tagh range are spatially confined to a small area in front of the mountains during the Paleogene, and thus deny the existence of long drainage systems southwardly flowing from the Altyn Tagh range to the southern study area.

(2) Based on the sediment distribution in study area, the spatial dissimilarities and similarities exhibited by detrital zircon age spectra and heavy minerals assemblages can be used to further testify the provenance inference. Signals only from presence or absence of the spectral age group (i.e., the late Paleozoic to early Mesozoic age group) in detrital zircon age spectra are not enough to determine the provenance.

(3) In the Xiaganchaigou Fm., a large sandy body with uniform distribution of detrital zircon ages and heavy minerals assemblages is sourced from the Qilian Mountains, implying that a large catchment area formed in the mountains under the control of intensive tectonic activity. The recycled late Paleozoic and Mesozoic sedimentary strata in the Qilian Mountains supply considerable late Paleozoic to early Mesozoic zircons. In addition, we consider that variation in proportions of the

spectral age groups (e.g., the late Paleozoic to early Mesozoic age group) in detrital zircon U-Pb age spectra need to be cautiously applied in provenance analysis of the Qaidam basin due to the complex rock types and intense tectonic activities of its surrounding mountains.

Supplementary Materials: The following are available online at <http://www.mdpi.com/2075-163X/10/10/854/s1>, Table S1: Data of the stratigraphic thickness, NTG ratios and conglomerate percentages, Table S2: Data of heavy mineral analysis, Table S3: Th/U ratios and detrital zircon U-Pb ages of the samples from the northern Qaidam Basin. Figure S1: The locations of drilled well.

Author Contributions: Conceptualization, J.Y. and S.Z.; methodology, J.Y. and S.Z.; validation, J.Y., S.Z., and Z.W.; formal analysis, J.Y., S.Z., and Z.W.; investigation, J.Y.; data curation, J.Y., S.Z., and Z.W.; writing—original draft preparation, J.Y. and S.Z.; writing—review and editing, J.Y., S.Z., and Z.W. All authors have read and agreed to the published version of the manuscript.

Funding: This research was funded by National geological survey project of China (Comprehensive survey of natural gas hydrate and petroleum resources in Domestic Permafrost Area, grant number: DD20190102).

Acknowledgments: The authors appreciate the prospective comments and suggestions from the reviewers and editors.

Conflicts of Interest: The authors declare no conflict of interest.

References

1. Cai, K.; Sun, M.; Yuan, C.; Xiao, W.; Zhao, G.; Long, X.; Wu, F. Carboniferous mantle-derived felsic intrusion in the Chinese Altai, NW China: Implications for geodynamic change of the accretionary orogenic belt. *Gondwana Res.* **2012**, *22*, 681–698. [[CrossRef](#)]
2. Wu, L.; Xiao, A.; Yang, S.; Wang, L.; Mao, L.; Wang, L.; Dong, Y.; Xu, B. Two-stage evolution of the Altyn Tagh Fault during the Cenozoic: New insight from provenance analysis of a geological section in NW Qaidam Basin, NW China. *Terra Nova* **2012**, *24*, 387–395. [[CrossRef](#)]
3. Zhuang, G.; Hourigan, J.K.; Ritts, B.D.; Kent-Corson, M.L. Cenozoic multiple-phase tectonic evolution of the northern Tibetan Plateau: Constraints from sedimentary records from Qaidam Basin, Hexi Corridor, and Subei basin, northwest China. *Am. J. Sci.* **2011**, *311*, 116–152. [[CrossRef](#)]
4. Bush, M.A.; Saylor, J.E.; Horton, B.K.; Nie, J. Growth of the Qaidam Basin during Cenozoic exhumation in the northern Tibetan Plateau: Inferences from depositional patterns and multiproxy detrital provenance signatures. *Lithosphere* **2016**, *8*, 58–82. [[CrossRef](#)]
5. Jian, X.; Guan, P.; Zhang, D.-W.; Zhang, W.; Feng, F.; Liu, R.-J.; Lin, S.-D. Provenance of Tertiary sandstone in the northern Qaidam Basin, northeastern Tibetan Plateau: Integration of framework petrography, heavy mineral analysis and mineral chemistry. *Sediment. Geol.* **2013**, *290*, 109–125. [[CrossRef](#)]
6. Rieser, A.B.; Neubauer, F.; Liu, Y.; Ge, X. Sandstone provenance of north-western sectors of the intracontinental Cenozoic Qaidam basin, western China: Tectonic vs. climatic control. *Sediment. Geol.* **2005**, *177*, 1–18. [[CrossRef](#)]
7. Sun, G.; Wang, M.; Guo, J.; Wang, Y.; Yang, Y. Geochemical Significance of Clay Minerals and Elements in Paleogene Sandstones in the Center of the Northern Margin of the Qaidam Basin, China. *Minerals* **2020**, *10*, 505. [[CrossRef](#)]
8. Cheng, F.; Fu, S.; Jolivet, M.; Zhang, C.; Guo, Z. Source to sink relation between the Eastern Kunlun Range and the Qaidam Basin, northern Tibetan Plateau, during the Cenozoic. *Geol. Soc. Am. Bull.* **2016**, *128*, 258–283. [[CrossRef](#)]
9. Cheng, F.; Jolivet, M.; Fu, S.; Zhang, C.; Zhang, Q.; Guo, Z. Large-scale displacement along the Altyn Tagh Fault (North Tibet) since its Eocene initiation: Insight from detrital zircon U-Pb geochronology and subsurface data. *Tectonophysics* **2016**, *677–678*, 261–279. [[CrossRef](#)]
10. Cheng, F.; Garzzone, C.N.; Mitra, G.; Jolivet, M.; Guo, Z.; Lu, H.; Li, X.; Zhang, B.; Zhang, C.; Zhang, H.; et al. The interplay between climate and tectonics during the upward and outward growth of the Qilian Shan orogenic wedge, northern Tibetan Plateau. *Earth-Sci. Rev.* **2019**, *198*, 102945. [[CrossRef](#)]
11. Lu, H.; Ye, J.; Guo, L.; Pan, J.; Xiong, S.; Li, H. Towards a clarification of the provenance of Cenozoic sediments in the northern Qaidam Basin. *Lithosphere* **2018**, *11*, 252–272. [[CrossRef](#)]

12. Song, B.; Zhang, K.; Hou, Y.; Ji, J.; Wang, J.; Yang, Y.; Yang, T.; Wang, C.; Shen, T. New insights into the provenance of Cenozoic strata in the Qaidam Basin, northern Tibet: Constraints from combined U-Pb dating of detrital zircons in recent and ancient fluvial sediments. *Palaeogeogr. Palaeoclimatol. Palaeocol.* **2019**, *533*, 109254. [[CrossRef](#)]
13. Wang, W.; Zheng, W.; Zhang, P.; Li, Q.; Kirby, E.; Yuan, D.; Zheng, D.; Liu, C.; Wang, Z.; Zhang, H.; et al. Expansion of the Tibetan Plateau during the Neogene. *Nat. Commun.* **2017**, *8*, 15887. [[CrossRef](#)] [[PubMed](#)]
14. Li, L.; Guo, Z.; Guan, S.; Zhou, S.; Wang, M.; Fang, Y.; Zhang, C. Heavy mineral assemblage characteristics and the Cenozoic paleogeographic evolution in southwestern Qaidam Basin. *Sci. China Earth Sci.* **2015**, *58*, 859–875. [[CrossRef](#)]
15. Li, L.; Wu, C.; Yu, X. Cenozoic evolution of the Altyn Tagh and East Kunlun fault zones inferred from detrital garnet, tourmaline and rutile in southwestern Qaidam Basin (Northern Tibetan Plateau). *Basin Res.* **2018**, *30*, 35–58. [[CrossRef](#)]
16. Nie, J.; Ren, X.; Saylor, J.E.; Su, Q.; Horton, B.K.; Bush, M.A.; Chen, W.; Pfaff, K. Magnetic polarity stratigraphy, provenance, and paleoclimate analysis of Cenozoic strata in the Qaidam Basin, NE Tibetan Plateau. *Geol. Soc. Am. Bull.* **2019**, *132*, 310–320. [[CrossRef](#)]
17. Jian, X.; Guan, P.; Zhang, W.; Feng, F. Geochemistry of Mesozoic and Cenozoic sediments in the northern Qaidam Basin, northeastern Tibetan Plateau: Implications for provenance and weathering. *Chem. Geol.* **2013**, *360–361*, 74–88. [[CrossRef](#)]
18. Weissmann, G.S.; Hartley, A.J.; Nichols, G.J.; Scuderi, L.A.; Olson, M.; Buehler, H.; Banteah, R. Fluvial form in modern continental sedimentary basins: Distributive fluvial systems. *Geology* **2010**, *38*, 39–42. [[CrossRef](#)]
19. Owen, A.; Hartley, A.J.; Ebinghaus, A.; Weissmann, G.S.; Santos, M.G.M. Basin-scale predictive models of alluvial architecture: Constraints from the Palaeocene–Eocene, Bighorn Basin, Wyoming, USA. *Sedimentology* **2019**, *66*, 736–763. [[CrossRef](#)]
20. Wang, Y.; Zheng, J.; Zheng, Y.; Liu, X.; Sun, G. Paleocene–Early Eocene uplift of the Altyn Tagh Mountain: Evidence from detrital zircon fission track analysis and seismic sections in the northwestern Qaidam Basin. *J. Geophys. Res-Sol Ea.* **2015**, *120*. [[CrossRef](#)]
21. Cheng, F.; Garzzone, C.N.; Jolivet, M.; Guo, Z.; Zhang, D.; Zhang, C.; Zhang, Q. Initial Deformation of the Northern Tibetan Plateau: Insights from Deposition of the Lulehe Formation in the Qaidam Basin. *Tectonics* **2019**, *38*, 741–766. [[CrossRef](#)]
22. Chang, H.; Li, L.; Qiang, X.; Garzzone, C.N.; Pullen, A.; An, Z. Magnetostratigraphy of Cenozoic deposits in the western Qaidam Basin and its implication for the surface uplift of the northeastern margin of the Tibetan Plateau. *Earth Planet. Sci. Lett.* **2015**, *430*, 271–283. [[CrossRef](#)]
23. Fang, X.; Zhang, W.; Meng, Q.; Gao, J.; Wang, X.; King, J.; Song, C.; Dai, S.; Miao, Y. High-resolution magnetostratigraphy of the Neogene Huaitoutala section in the eastern Qaidam Basin on the NE Tibetan Plateau, Qinghai Province, China and its implication on tectonic uplift of the NE Tibetan Plateau. *Earth Planet. Sci. Lett.* **2007**, *258*, 293–306. [[CrossRef](#)]
24. Lu, H.; Xiong, S. Magnetostratigraphy of the Dahonggou section, northern Qaidam Basin and its bearing on Cenozoic tectonic evolution of the Qilian Shan and Altyn Tagh Fault. *Earth Planet. Sci. Lett.* **2009**, *288*, 539–550. [[CrossRef](#)]
25. Sun, Z.; Yang, Z.; Pei, J.; Ge, X.; Wang, X.; Yang, T.; Li, W.; Yuan, S. Magnetostratigraphy of Paleogene sediments from northern Qaidam Basin, China: Implications for tectonic uplift and block rotation in northern Tibetan plateau. *Earth Planet. Sci. Lett.* **2005**, *237*, 635–646. [[CrossRef](#)]
26. Yang, F.; Ma, Z.; Xu, T.; Ye, S. A tertiary paleomagnetic stratigraphic profile in Qaidam Basin. *Acta Pet. Sin.* **1992**, *13*, 97–101, (In Chinese with English abstract).
27. Zhang, W. The High Precise Cenozoic Magnetostratigraphy of the Qaidam Basin and Uplift of the Northern Tibetan Plateau. Ph.D. Thesis, Lanzhou University, Lanzhou, China, 2006.
28. Song, B.; Spicer, R.A.; Zhang, K.; Ji, J.; Farnsworth, A.; Hughes, A.C.; Yang, Y.; Han, F.; Xu, Y.; Spicer, T.; et al. Qaidam Basin leaf fossils show northeastern Tibet was high, wet and cool in the early Oligocene. *Earth Planet. Sci. Lett.* **2020**, *537*, 116175. [[CrossRef](#)]
29. Ke, X.; Ji, J.; Zhang, K.; Kou, X.; Song, B.; Wang, C. Magnetostratigraphy and Anisotropy of Magnetic Susceptibility of the Lulehe Formation in the Northeastern Qaidam Basin. *Acta Geol. Sin.* **2013**, *87*, 576–587.
30. Gehrels, G.E.; Yin, A.; Wang, X.-F. Detrital-zircon geochronology of the northeastern Tibetan plateau. *Geol. Soc. Am. Bull.* **2003**, *115*, 881–896. [[CrossRef](#)]

31. Gehrels, G.E.; Yin, A.; Wang, X.-F. Magmatic history of the northeastern Tibetan Plateau. *J. Geophys. Res. Solid Earth* **2003**, *108*, 2423. [[CrossRef](#)]
32. Song, S.; Niu, Y.; Su, L.; Zhang, C.; Zhang, L. Continental orogenesis from ocean subduction, continent collision/subduction, to orogen collapse, and orogen recycling: The example of the North Qaidam UHPM belt, NW China. *Earth-Sci. Rev.* **2014**, *129*, 59–84. [[CrossRef](#)]
33. Yin, A.; Harrison, T.M. Geologic evolution of the Himalayan-Tibetan orogen. *Annu. Rev. Earth Pl. Sc.* **2000**, *28*, 211–280. [[CrossRef](#)]
34. Chen, X.; Gehrels, G.; Yin, A.; Li, L.; Jiang, R. Paleozoic and Mesozoic Basement Magmatism of Eastern Qaidam Basin, Northern Qinghai-Tibet Plateau: LA-ICP-MS Zircon U-Pb Geochronology and its Geological Significance. *Acta Geol. Sin.* **2012**, *86*, 350–369.
35. Luo, K. *The Evolution of Carboniferous-Triassic Basin in Tuolai River on the Northern Margin of Center Qilian Block*; China University of Geosciences (Beijing): Beijing, China, 2015; (In Chinese with English Abstract).
36. Wu, L. *The Detrital-Zircon U-Pb Dating and Provenance Analysis for the Triassic Sandstone in Qilian Shan, Northeastern Margin of the Tibetan Plateau*; China University of Geosciences (Beijing): Beijing, China, 2013; (In Chinese with English Abstract).
37. Zhao, J.; Zeng, X.; Tian, J.; Hu, C.; Wang, D.; Yan, Z.; Wang, K.; Zhao, X. Provenance and paleogeography of the Jurassic Northwestern Qaidam Basin (NW China): Evidence from sedimentary records and detrital zircon geochronology. *J. Asian Earth Sci.* **2020**, *190*, 104060. [[CrossRef](#)]
38. Wang, C.; Liu, L.; Xiao, P.-X.; Cao, Y.-T.; Yu, H.-Y.; Meert, J.G.; Liang, W.-T. Geochemical and geochronologic constraints for Paleozoic magmatism related to the orogenic collapse in the Qimantagh–South Altyn region, northwestern China. *Lithos* **2014**, *202–203*, 1–20. [[CrossRef](#)]
39. Chen, X.; Gehrels, G.; Yin, A.; Zhou, Q.; Huang, P. Geochemical and Nd–Sr–Pb–O isotopic constrains on Permo–Triassic magmatism in eastern Qaidam Basin, northern Qinghai-Tibetan plateau: Implications for the evolution of the Paleo-Tethys. *J. Asian Earth Sci.* **2015**, *114*, 674–692. [[CrossRef](#)]
40. Dong, Y.; He, D.; Sun, S.; Liu, X.; Zhou, X.; Zhang, F.; Yang, Z.; Cheng, B.; Zhao, G.; Li, J. Subduction and accretionary tectonics of the East Kunlun orogen, western segment of the Central China Orogenic System. *Earth-Sci. Rev.* **2018**, *186*, 231–261. [[CrossRef](#)]
41. Mo, X.; Luo, Z.; Deng, J.-f.; Yu, X.; LIU, C.; Chen, H.; Yuan, W.; Liu, Y. Granitoids and Crustal Growth in the East-Kunlun Orogenic Belt (in Chinese with English abstract). *Acta Metall. Sin.* **2007**, *13*, 403–414.
42. Mange, M.A.; Maurer, H.F.W. *Heavy Minerals in Color*; Chapman and Hall: London, UK, 1992.
43. Liu, Y.; Hu, Z.; Li, M.; Gao, S. Applications of LA-ICP-MS in the elemental analyses of geological samples. *Chin. Sci. Bull.* **2013**, *58*, 3863–3878. [[CrossRef](#)]
44. Wiedenbeck, M.; Allé, P.; Corfu, F.; Griffin, W.L.; Meier, M.; Oberli, F.; Quadt, A.V.; Roddick, J.C.; Spiegel, W. Three natural zircon standards for U-Th-Pb, Lu-Hf, trace element and REE analyses. *Geostandard. Newslett.* **1995**, *19*, 1–23. [[CrossRef](#)]
45. Ludwig, K.R. User’s Manual for Isoplot/Ex, Version 3.00, A Geochronological Toolkit for Microsoft Excel. *Berkeley Geochronol. Cent. Spec. Publ.* **2003**, *4*, 1–70.
46. Yuan, H.; Gao, S.; Liu, X.; Li, H.; Günther, D.; Wu, F. Accurate U-Pb Age and Trace Element Determinations of Zircon by Laser Ablation-Inductively Coupled Plasma-Mass Spectrometry. *Geostand. Geoanal. Res.* **2004**, *28*, 353–370. [[CrossRef](#)]
47. Liu, S.; Li, J.; Stockli, D.F.; Song, C.; Guo, B.; Stockli, L.D.; Ma, Z.; Li, X.; Peng, T. Reappraisal of Miocene eolian deposition in Tianshui Basin, China, based on an investigation of stratigraphy and provenance. *Geol. Soc. Am. Bull.* **2019**, *131*, 1312–1332. [[CrossRef](#)]
48. Belousova, E.A.; Griffin, W.L.; O’Reilly, S.Y.; Fisher, N.I. Igneous zircon: Trace element composition as an indicator of source rock type. *Contrib. Mineral. Petr.* **2002**, *143*, 602–622. [[CrossRef](#)]
49. Su, N.N.; Jin, Z.K.; Song, F.; Gu, J.F.; Zhang, W.D. Sedimentary facies of the Paleogene in Qaidam Basin. *J. China Univ. Pet.* **2014**, *38*, 1–9, (In Chinese with English abstract).
50. Ji, J.; Zhang, K.; Clift, P.D.; Zhuang, G.; Song, B.; Ke, X.; Xu, Y. High-resolution magnetostratigraphic study of the Paleogene-Neogene strata in the Northern Qaidam Basin: Implications for the growth of the Northeastern Tibetan Plateau. *Gondwana Res.* **2017**, *46*, 141–155. [[CrossRef](#)]
51. Fu, L.; Guan, P.; Zhao, W.; Wang, M.; Zhang, Y.; Lu, J. Heavy mineral feature and provenance analysis of Paleogene Lulehe Formation in Qaidam Basin. *Acta Petrol. Sin.* **2013**, *29*, 2867–2875, (In Chinese with English abstract).

52. Yin, A.; Dang, Y.-Q.; Zhang, M.; Chen, X.-H.; McRivette, M.W. Cenozoic tectonic evolution of the Qaidam basin and its surrounding regions (Part 3): Structural geology, sedimentation, and regional tectonic reconstruction. *Geol. Soc. Am. Bull.* **2008**, *120*, 847–876. [[CrossRef](#)]
53. Tang, W.; Zhang, Z.; Li, J.; Li, K.; Chen, Y.; Guo, Z. Late Paleozoic to Jurassic tectonic evolution of the Bogda area (northwest China): Evidence from detrital zircon U-Pb geochronology. *Tectonophysics* **2014**, *626*, 144–156. [[CrossRef](#)]
54. He, P.; Song, C.; Wang, Y.; Meng, Q.; Chen, L.; Yao, L.; Huang, R.; Feng, W.; Chen, S. Cenozoic deformation history of the Qilian Shan (northeastern Tibetan Plateau) constrained by detrital apatite fission-track thermochronology in the northeastern Qaidam Basin. *Tectonophysics* **2018**, *749*, 1–11. [[CrossRef](#)]
55. Jian, X.; Guan, P.; Zhang, W.; Liang, H.; Feng, F.; Fu, L. Late Cretaceous to early Eocene deformation in the northern Tibetan Plateau: Detrital apatite fission track evidence from northern Qaidam basin. *Gondwana Res.* **2018**, *60*, 94–104. [[CrossRef](#)]
56. Yin, A.; Dang, Y.-Q.; Wang, L.-C.; Jiang, W.-M.; Zhou, S.-P.; Chen, X.-H.; Gehrels, G.E.; McRivette, M.W. Cenozoic tectonic evolution of Qaidam basin and its surrounding regions (Part 1): The southern Qilian Shan-Nan Shan thrust belt and northern Qaidam basin. *Geol. Soc. Am. Bull.* **2008**, *120*, 813–846. [[CrossRef](#)]
57. Wang, Y.T.; Sun, G.Q.; Yang, Y.H.; Wang, M.; Ma, F.Q.; Zhang, C.J.; Zhao, J.; Shi, J.A. U-Pb geochronology analysis of detrital zircons in the Paleogene lower Xiaganchaigou formation in the northern Mahai area, northern margin of Qaidam Basin. *J. Lanzhou Univ.* **2019**, *55*, 141–148, 157, (In Chinese with English abstract).
58. Hartley, A.J.; Weissmann, G.S.; Nichols, G.J.; Warwick, G.L. Large Distributive Fluvial Systems: Characteristics, Distribution, and Controls on Development. *J. Sediment. Res.* **2010**, *80*, 167–183. [[CrossRef](#)]
59. He, P.; Song, C.; Wang, Y.; Chen, L.; Chang, P.; Wang, Q.; Ren, B. Cenozoic exhumation in the Qilian Shan, northeastern Tibetan Plateau: Evidence from detrital fission track thermochronology in the Jiuquan Basin. *J. Geophys. Res. Solid Earth* **2017**, *122*, 6910–6927.
60. Jolivet, M.; Brunel, M.; Seward, D.; Xu, Z.; Yang, J.; Roger, F.; Tapponnier, P.; Malavieille, J.; Arnaud, N.; Wu, C. Mesozoic and Cenozoic tectonics of the northern edge of the Tibetan plateau: Fission-track constraints. *Tectonophysics* **2001**, *343*, 111–134. [[CrossRef](#)]
61. Bao, J.; Wang, Y.; Song, C.; Feng, Y.; Hu, C.; Zhong, S.; Yang, J. Cenozoic sediment flux in the Qaidam Basin, northern Tibetan Plateau, and implications with regional tectonics and climate. *Glob. Planet. Chang.* **2017**, *155*, 56–69. [[CrossRef](#)]



© 2020 by the authors. Licensee MDPI, Basel, Switzerland. This article is an open access article distributed under the terms and conditions of the Creative Commons Attribution (CC BY) license (<http://creativecommons.org/licenses/by/4.0/>).